frontiers in Chemistry

ORIGINAL RESEARCH
published: 19 August 2021
doi: 10.3389/fchem.2021.734460

Achieving Selective and Efficient Electrocatalytic Activity for CO_2 Reduction on N-Doped Graphene

Xiaoxu Sun *

Jiangsu Key Laboratory of New Power Batteries, School of Chemistry and Materials Science, Nanjing Normal University, Nanjing, China

The CO_2 electrochemical reduction reaction (CO_2RR) has been a promising conversion method for CO_2 utilization. Currently, the lack of electrocatalysts with favorable stability and high efficiency hindered the development of CO_2RR. Nitrogen-doped graphene nanocarbons have great promise in replacing metal catalysts for catalyzing CO_2RR. By using the density functional theory (DFT) method, the catalytic mechanism and activity of CO_2RR on 11 types of nitrogen-doped graphene have been explored. The free energy analysis reveals that the zigzag pyridinic N- and zigzag graphitic N-doped graphene possess outstanding catalytic activity and selectivity for HCOOH production with an energy barrier of 0.38 and 0.39 eV, respectively. CO is a competitive product since its free energy lies only about 0.20 eV above HCOOH. The minor product is CH_3OH and CH_4 for the zigzag pyridinic N-doped graphene and HCHO for zigzag graphitic N-doped graphene, respectively. However, for Z-pyN, CO_2RR is passivated by too strong HER. Meanwhile, by modifying the pH value of the electrolyte, Z-GN could be selected as a promising nonmetal electrocatalyst for CO_2RR in generating HCOOH.

Keywords: density functional theory, N-doped graphene, CO_2 reduction reaction, catalytic activity, Gibbs free energy

OPEN ACCESS

Edited by:
Zhaofu Zhang,
University of Cambridge,
United Kingdom

Reviewed by:
Liu Xuefei,
Guizhou Normal University, China
Ziheng Lu,
University of Cambridge,
United Kingdom

***Correspondence:**
Xiaoxu Sun
xxsun@ciac.ac.cn

Specialty section:
This article was submitted to Theoretical and Computational Chemistry, a section of the journal Frontiers in Chemistry

Received: *01 July 2021*
Accepted: *12 July 2021*
Published: *19 August 2021*

Citation:
Sun X (2021) Achieving Selective and Efficient Electrocatalytic Activity for CO_2 Reduction on N-Doped Graphene. Front. Chem. 9:734460. doi: 10.3389/fchem.2021.734460

INTRODUCTION

As one of the greenhouse gases, the continual accumulation of CO_2 causes global warming, which significantly hinders the sustainable development of human society (Thomas et al., 2004; Lewis et al., 2006; Cook et al., 2010). The unbalanced CO_2 emission and consumption is becoming a pressing issue (Kondratenko et al., 2013; Appel et al., 2013). In this aspect, CO_2 electrochemical reduction reaction (CO_2RR) by using the renewable energy sources (Yi et al., 2019; Wang et al., 2020; Lu et al., 2021) offers a promising way to produce fuels and value-added chemicals. Up to now, the major obstacle for CO_2RR is the lack of electrocatalysts with high stability and efficiency. Particularly, the cathode electrocatalyst materials play a key role in the complicated product distribution of CO_2RR (Lim et al., 2014; Zhu et al., 2016). Therefore, searching for suitable electrocatalysts for CO_2RR is one of the hot topics in recent years. Till now, a lot of electrocatalysts for CO_2RR have been studied, including noble metals (Zhu et al., 2013; Kang et al., 2014; Gao et al., 2015; Kim et al., 2015), base metals (Hori et al., 1985; Hori et al., 1986; Nie et al., 2013; Zhang et al., 2014a), alloys (Kim et al., 2014; Bai et al., 2017), and metal oxides (Lee et al., 2015; Ren et al., 2015). It is well known that Ag and Au are prone to produce CO *via* the two-electron reaction pathway (Zhu et al., 2013; Kim et al., 2015). In addition, Cu is recognized as a state-of-the-art CO_2RR catalyst for generating multi-electron products, such as CO, HCOOH, CH_3OH, and CH_4 (Hori et al., 1985; Hori et al., 1986; Nie

et al., 2013). However, the high cost, low efficiency due to the competitive hydrogen evolution reaction (HER), and high overpotential restrict their practical implementation and industrial-scale development in CO_2RR (Lim et al., 2014).

To solve the above issues, metal-free electrocatalysts based on carbon materials have been studied, owing to their low cost, high stability, outstanding mechanical flexibility, and superior structural durability. The introduction of heteroatoms (such as N, B, and S) could not only modify the electronic structure of carbon materials but also contribute to take advantage of the existing defects appropriately (Wang X. et al., 2014). For N-doped carbon nanofibers (NCNFs), it shows negligible overpotential (0.17 V) and 13 times higher current density than bulk Ag catalyst for CO_2RR (Kumar et al., 2013). In addition, N-doped carbon nanotubes (NCNTs) (Sharma et al., 2015), N-doped nanoporous carbon–carbon nanotube composite membrane (HNCM/CNT) (Wang et al., 2017), and polyethylenimine functionalized NCNTs have been proven to be highly active and stable electrocatalysts for CO_2RR (Zhang et al., 2014b). Remarkably, N-doped graphene possesses excellent durability in the CO_2RR process, achieving a maximum faradaic efficiency (FE) of 73% for formate with overpotential of 0.84 V (Wang et al., 2016). N-doped graphene quantum dots (NGQDs) could catalyze carbon dioxide into multicarbon hydrocarbons and oxygenates at high FE (up to 90%), with excellent selectivity (45% for ethylene and ethanol conversions) (Wu et al., 2016).

With respect to the active sites of nitrogen-doped carbon materials for CO_2RR, it is a controversial issue among the pyridinic N, pyrrolic N, graphitic N, and the C adjacent to N. Generally, these potential active sites coexist in the carbon materials, which adds to the difficulty in identifying the active site. A theoretical study indicates that for CO_2 electroreduction to CO on NCNTs, the optimal active site is pyridinic N, followed by pyrrolic N and graphitic N (Wu et al., 2015). Another study about CO_2RR on NCNTs emphasizes that the presence of graphitic and pyridinic N defects remarkably increases the selectivity toward CO formation and decreases the absolute overpotential (Sharma et al., 2015). For N-doped graphene-like material/carbon paper electrodes (NGM/CP), the FE is as high as 93.5% in producing CH_4, which is ascribed to the reactive pyridinic and pyrrolic N sites (Sun et al., 2016). A theoretical study suggested that COOH production on pyrrolic N3 is downhill by −0.21 eV, while it is uphill for pyridinic and graphitic N (Liu et al., 2016). Overall, both the experimental and theoretical studies indicate that N-doped carbon materials show significant catalytic performance of CO_2RR.

Inspired by these studies, we studied CO_2RR on N-doped graphene from the perspective of theoretical calculation in this work. To make a systematic comparison, N was doped into graphene at in-plane, zigzag edge, armchair edge, and pyrrolic edge sites, respectively. It would contribute to identifying the most dominant structure and providing a valuable design strategy for further activity enhancement in the experiment. In this study, the first-principle calculation has been performed to uncover the CO_2RR reaction pathways and electrocatalytic activity on different edges of N-doped (zigzag edge, armchair edge, and pyrrolic edge) graphene structures within a unified thermodynamic reaction scheme.

COMPUTATIONAL METHODS AND MODELS

Methods

The geometry optimization and energy calculations were performed within the density functional theory (DFT) framework (Kohn and Sham, 1965) by using the Vienna *ab initio* simulation package (VASP) (Kresse and Furthmüller, 1996a). The ion–electron interaction was described by the projector-augmented wave (PAW) potentials (Blöchl, 1994). The generalized gradient approximation parameterized by Perdew, Burke, and Ernzerhof was utilized as the exchange-correlation functional (Perdew et al., 1996). The kinetic energy cutoff of 400 eV was adopted for the plane-wave expansion. The armchair-edged ribbon, zigzag-edged ribbon, and periodic graphene slab were sampled with 4 × 1 × 1, 1 × 4×1, and 4 × 4 × 1 Monkhorst−Pack k-point grids (Delley, 2000), respectively. During the geometry optimization, all atoms were relaxed until the total energy was converged to 1.0×10^{-5} eV/atom, and the force was converged to 0.01 eV/Å. In addition, we considered the van der Waals (vdW) interactions by employing the semiempirical DFT-D2 forcefield approach (Grimme, 2006).

Models

The lattice parameters of 8.52 Å × 24.6 Å and 25.6 Å × 9.84 Å were set to model the armchair-edged graphene nanoribbon (including pyrrolic edge) and zigzag-edged graphene nanoribbon, respectively. The lattice parameters of 9.84 × 9.84Å were adopted to model the periodic graphene slab. Perpendicular to all graphene structures, a vacuum layer of 15 Å was set, which was sufficiently large to minimize the image interactions.

The adsorption energy(ΔE_{ads})of adsorbates was defined as follows:

$$\Delta E_{ads} = E_{substrate+adsorbate} - (E_{substrate} + E_{adsorbate}), \quad (1)$$

where $E_{substrate+adsorbate}$ is the total energy of the substrate with adsorbed molecules. $E_{substrate}$ and $E_{adsorbate}$ are the energy of the isolated substrate and free molecule, respectively.

Reaction Free Energy

The computational hydrogen electrode (CHE) model (Norskov et al., 2004) was adopted to evaluate the free energy change during the CO_2RR process. In the CHE model, the hydrogen atom is in equilibrium with the proton/electron pair at 298.15 K and 1 atm of pressure. In other words, the half chemical potential of gas-phase H_2 is equal to that of a proton/electron pair at 0 V in an aqueous solution.

The Gibbs free energy change (ΔG) for each elementary CO_2RR step involving proton/electron pair transfer was calculated by the expression (Norskov et al., 2004; Zuluaga and Stolbov, 2011):

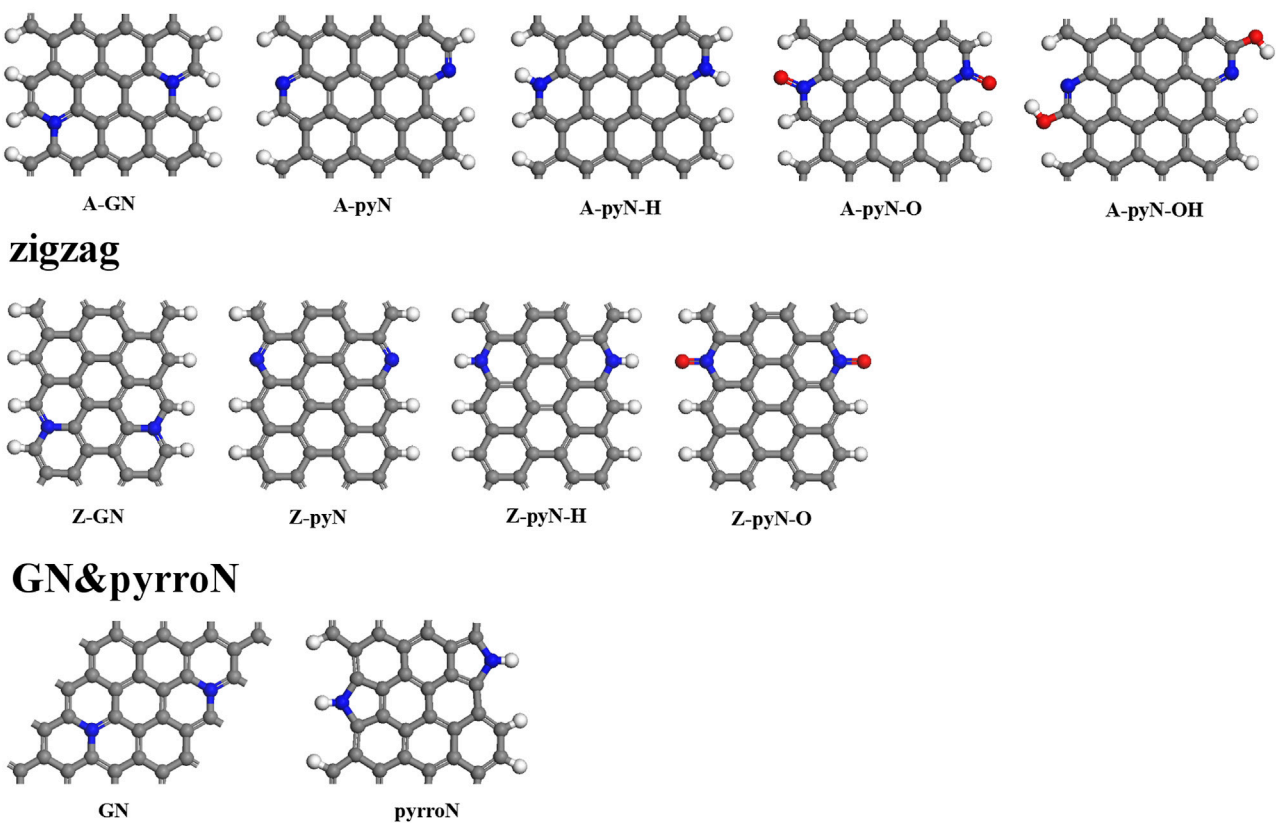

FIGURE 1 | The structures of N-doped graphene. The gray, blue, white, and red balls represent C, N, H, and O atoms, respectively.

$$\Delta G = \Delta E + \Delta ZPE - T\Delta S + \Delta Gu + \Delta G_{pH}, \quad (2)$$

where ΔE is the change of reaction energy based on DFT calculations. ΔZPE and ΔS are the change of zero-point energy and entropy, respectively. T refers to the temperature (298.15 K). The zero-point energy (*ZPE*) of adsorbates has been calculated from the vibrational frequencies. For the free molecules (CO_2, CO, HCOOH, CH_4, CH_3OH, *etc.*) the vibrational frequencies and entropies are obtained from the NIST database (http://webbook.nist.gov/chemistry/). ΔG_U = -*n*eU, where *n* is the number of transferred electrons, *e* is the elementary charge of an electron, and U is the electrode potential vs. RHE. $\Delta G_{pH=}$ 2.303 k_BT *pH, k_B is the Boltzmann constant. In this work, the value of pH was set as 0 for the acid medium (Faccio et al., 2010; Shang et al., 2010). Approximate solvation corrections with a dielectric constant of ε = 80 are applied for the simulation of an aqueous environment (Mathew et al., 2019).

RESULT AND DISCUSSION

Adsorption of the Key Intermediates

In previous reports, the N-doped graphene materials have been widely studied as ORR electrocatalysts, which showed better stability and tolerance to methanol crossover effect than commercial Pt/C catalyst (Geng et al., 2011; Lin et al., 2013; Gong et al., 2009; Qu et al., 2010). Under different temperatures, the synthesizability of each type of the N-doped graphene materials is different. It is relatively easy to synthesize different types of N-doped graphene by controlling the temperature (Lin et al., 2013). The studied structures include five N-doped armchair graphene types, four N-doped zigzag graphene types, in-plane graphitic N (GN), and pyrrolic edge N (PyrroN)-doped graphene. For N-doped armchair graphene, it includes graphitic N (A-GN), pyridinic N (A-pyN), hydrogenated pyridinic N (A-pyN-H), oxidized pyridinic N (A-pyN-O), and pyridinic N hydroxide (A-pyN-OH), as shown in **Figure 1**. For N-doped zigzag graphene, four structures are considered, i.e., graphitic N (Z-GN), pyridinic N (Z-pyN), hydrogenated pyridinic N (Z-pyN-H), and oxidized pyridinic N (Z-pyN-O). These doped structures could be generated at high temperatures in the pyrolysis process of N-containing compounds (Wu et al., 2011; Li et al., 2012; Wang Q. et al., 2014; Holby et al., 2014).

During the CO_2RR process on the studied compounds, the intermediates mainly include CO_2, COOH, HCOO, HCOOH, CO + H_2O, COHOH, H_2COO, and COH + H_2O. By exploring different adsorption sites (N and its adjacent carbon atoms),

TABLE 1 | The calculated adsorption energies (E_{ads}, eV) and the shortest distances (d, Å) between the intermediate and N-doped graphene.

	*CO_2		*COOH		*HCOO		*HCOOH		*CO	
	E_{ads}	D	E_{ads}	d	E_{ads}	d	E_{ads}	d	E_{ads}	d
A-GN	−0.13	3.14	−1.26	1.57	—	—	−0.12	2.23	−0.13	3.12
A-pyN	−0.10	3.08	−1.51	1.42	−0.92	1.52	−0.33	1.73	−0.04	3.22
A-pyN-H	−0.10	3.10	−0.20	1.53	—	—	−0.05	1.92	−0.03	3.17
A-pyN-O	−0.11	3.32	−0.95	1.56	−1.29	1.50	−0.40	1.62	−0.08	3.26
A-pyN-OH	−0.11	3.12	−0.96	1.40	−0.84	1.54	−0.24	1.63	−0.07	3.19
Z-GN	−0.10	3.25	−1.99	1.58	−1.87	1.50	−0.16	2.02	−0.10	3.14
Z-pyN	−0.09	3.36	−2.48	1.41	—	—	−0.43	1.64	−0.26	1.37
Z-pyN-H	−0.09	3.19	−0.43	1.58	—	—	−0.13	2.00	−0.09	3.17
Z-pyN-O	−0.08	3.19	−0.59	1.55	—	—	−0.06	2.39	−0.10	3.20
GN	−0.06	3.11	0.34	1.61	—	—	−0.10	2.22	−0.12	3.14
PyrroN	−0.10	3.03	—	—	—	—	—	—	—	—

The "" denotes the adsorption state of the species.*

the most favorable adsorption configurations and sites are obtained (**Supplementary Figures 1–8**). Since the two main reactions on various N-doped graphene are HCOOH and CO generation pathways, we focus on the adsorption energies of CO_2, COOH, HCOO, HCOOH, and CO as listed in **Table 1**, together with the bond distance between the adsorbed intermediates and catalyst surface. It is seen that the adsorption of CO_2 molecule is weak all the time (-0.06 eV~ -0.13 eV), and linear structure is maintained above the surface. To achieve high selectivity for HCOOH or CO, COOH (or HCOO) should be adsorbed strongly, but HCOOH or CO should be adsorbed weakly for desorption. Therefore, strong COOH (HCOO) binding but weak HCOOH (CO) adsorption is essential for the formation of HCOOH or (CO) (Sharma et al., 2015; Wu et al., 2015).

As shown in **Supplementary Figures 2, 3**, COOH could not be absorbed on GN and PyrroN, and is weakly adsorbed on A-pyN-H (-0.20 eV), Z-pyN-H (-0.43 eV), and Z-pyN-O (−0.59 eV) (**Table 1**). For the remaining structures, the adsorption of COOH is relatively strong, with the adsorption energy ranging from −0.95 to −2.48 eV. However, HCOO exists only on four N-doped graphene structures, that is, A-pyN, A-pyN-O, A-pyN-OH, and Z-GN. The adsorption energies for the four structures are in the range of −1.87 eV~ −0.84 eV (**Table 1**).

For HCOOH, the adsorption energies for the studied compounds are in the range of −0.43 ~ −0.06 eV, which are relatively weak and facilitate its desorption from the catalyst surface. Similar to the HCOOH molecule, the adsorption energies of CO are in the range of −0.26 ~ −0.03 eV (**Table 1**).

Reaction Mechanism

The possible reaction pathways for the studied compounds are summarized in **Figure 2**. Based on the computational hydrogen electrode (CHE) model (Norskov et al., 2004), the limiting potential is obtained by $U_L = -\Delta G_{MAX}/e$, where ΔG_{MAX} denotes the maximum free energy difference between the two successive reaction steps. The reduction step corresponding to the limiting potential is defined as the potential determining step (PDS).

N-Doped Armchair Graphene Nanoribbons

As shown in **Figures 2A–E**, the energy of CO_2 increases by 0.25–0.37 eV from the free molecule to the adsorbed state. After CO_2 is adsorbed on the catalyst surface, it would be hydrogenated by ($H^+ + e^-$) pair. The formation of an O-H bond would produce COOH, while the formation of the C-H bond would generate the HCOO intermediate.

The reaction of $CO_2+H^++e^-\rightarrow$*COOH on A-GN, A-pyN, A-pyN-H, A-pyN-O, and A-pyN-OH is uphill by 1.16, 0.84, 2.14, 1.38, and 1.41 eV, respectively. For $CO_2+ H^++e^-\rightarrow$*HCOO, the energy increases by 1.73, 1.38, and 1.81 eV for A-pyN, A-pyN-O, and A-pyN-OH, respectively.

The hydrogenation of COOH would generate COHOH, HCOOH, and CO + H_2O. Due to the large energy increase for producing COHOH, that is, 1.55, 0.96, and 1.26 eV for A-GN, A-pyN, and A-pyN-OH, respectively, further discussion is omitted. In COOH, if the OH moiety binds (H^++e^-), it would produce CO + H_2O. If the carbon atom in COOH binds (H^++e^-), it would produce HCOOH. The production of HCOOH and CO is all thermodynamically downhill.

Similarly, the hydrogenation of HCOO may produce H_2COO and HCOOH. As *HCOO→*H_2COO step is endothermic with a large free energy increase (0.88 eV for A-pyN, 0.93 eV for A-pyN-O, and 1.86 eV for A-pyN-OH), further discussion is not provided. Thus, the final product from HCOO is HCOOH.

As illustrated in **Figures 2A–E**, the COOH intermediate has better performance in producing HCOOH than HCOO. For $CO_2\rightarrow$ *$CO_2\rightarrow$*COOH→*HCOOH/*CO, the PDS is *$CO_2\rightarrow$*COOH (**Table 2**), which is in agreement with the previous study (Wu et al., 2015). According to the free energy barrier (**Figures 2A–E**), A-pyN exhibits the highest catalytic activity toward HCOOH with a free energy barrier of 0.84 eV (**Figure 2B**). The order of catalytic activity for COOH to HCOOH/CO is A-pyN > A-GN > A-pyN-O > A-pyN-OH > A-pyN-H. In addition, $CO_2\rightarrow$ *$CO_2\rightarrow$*COOH→*CO+*H_2O is the secondary pathway with slightly larger endothermic energy than $CO_2\rightarrow$ *$CO_2\rightarrow$*COOH→*HCOOH.

N-Doped Zigzag Graphene Nanoribbons

The reaction pathways on N-doped zigzag graphene nanoribbons (**Figures 2F–I**) are similar to those on N-doped armchair

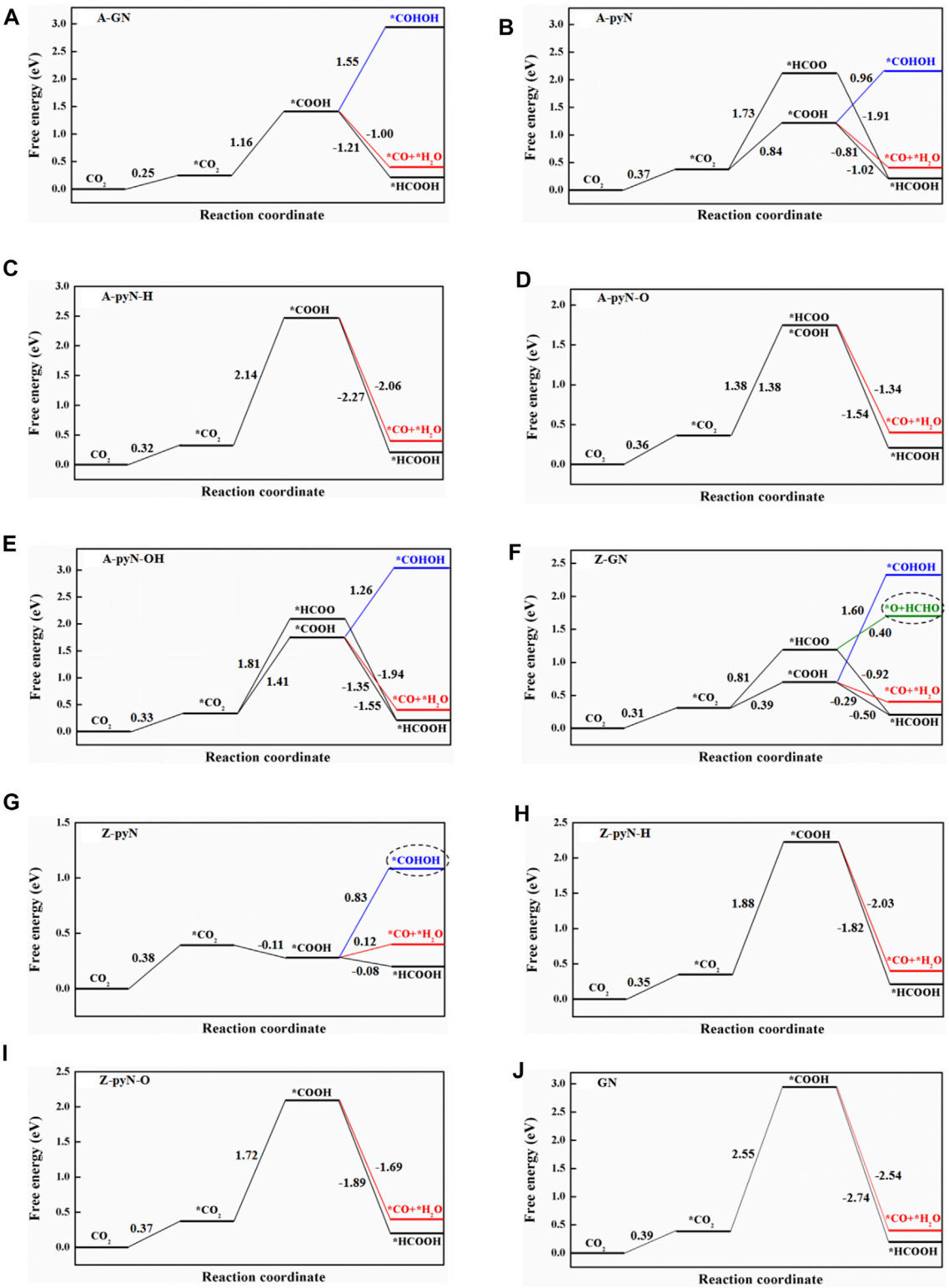

FIGURE 2 | The free energy change for reaction pathways of CO_2RR on various N-doped graphene. **(A)** A-GN, **(B)** A-pyN, **(C)** A-pyN-H, **(D)** A-pyN-O, **(E)** A-pyN-OH, **(F)** Z-GN, **(G)** Z-pyN, **(H)** Z-pyN-H, **(I)** Z-pyN-O, **(J)** GN.

TABLE 2 | Potential determining steps (PDSs), limiting potentials (U_L/V), and overpotentials (η/V) for CO_2RR on Z-GN and Z-pyN. U_0 is the equilibrium potential. Comparison has been made with previous studies. U_L, U_0, and η are all vs. the RHE.

	PDS	U_L	U_0	η	Product
Z-GN	$*CO_2+H^+ + e^- \rightarrow *COOH$	−0.39	−0.25	0.14	HCOOH
Z-GN	$*CO_2+H^+ + e^- \rightarrow *COOH$	−0.39	−0.11	0.28	CO
Z-GN	$*CO_2+H^+ + e^- \rightarrow *HCOO$	−0.81	−0.07	0.74	HCHO
Z-pyN	$CO_2+H^+ + e^- \rightarrow *CO_2$	−0.38	−0.25	0.13	HCOOH
Z-pyN	$CO_2+H^+ + e^- \rightarrow *CO_2$	−0.38	−0.11	0.27	CO
Z-pyN	$*COOH + H^+ + e^- \rightarrow *COHOH$	−0.83	0.02	0.81	CH_3OH
Z-pyN	$*COOH + H^+ + e^- \rightarrow *COHOH$	−0.83	0.17	0.66	CH_4
PyrroN3	$*COOH + H^+ + e^- \rightarrow HOOH$	−0.44	—	—	HCOOH
Edge-2gN	$CO_2+H^+ + e^- \rightarrow *COOH$	−0.52	—	—	CO

The "" denotes the adsorption state of the species.*

graphene nanoribbons. The HCOO intermediate could only stably exist on Z-GN among these N-doped zigzag graphene nanoribbons. To produce HCOOH, the $CO_2 \rightarrow *CO_2 \rightarrow *COOH \rightarrow *HCOOH$ pathway is more favorable than the $CO_2 \rightarrow *CO_2 \rightarrow *HCOO \rightarrow *HCOOH$ pathway (**Figure 2F**). In particular, on Z-GN, the hydrogenation of HCOO generates not only HCOOH but also O + HCHO with an energy barrier of 0.40 eV (**Figure 2F**). As illustrated in **Figure 3**, after the formation of O + HCOO, the remaining O atom could be easily hydrogenated into water due to the downhill process. The PDS for producing HCHO is the HCOO formation step with U_L = -0.81 V.

For the $*CO_2 \rightarrow *COOH$ step, it occurred on Z-GN and Z-pyN most easily, in which the energy is uphill by 0.39 eV for Z-GN and downhill by -0.11 eV for Z-pyN, respectively (**Figures 2F,G**). While for the other two structures, large uphill energy barriers are required, that is, 1.88 eV for Z-pyN-H and 1.72 eV for Z-pyN-O, respectively. After the formation of COOH, its hydrogenation may generate HCOOH, CO + H_2O, or COHOH, in which the formation of HCOOH is the most favorable, followed by CO + H_2O and COHOH. Our calculations indicated that the COOH intermediate on Z-pyN needs an energy barrier of 0.83 eV to form COHOH (**Figure 4**). After the formation of COHOH, an energy increase of 0.41 eV is required to produce COH + H_2O. The further hydrogenation of COH is relatively easy due to the downhill energy process to release the two competitive final products, that is, CH_3OH and CH_4. A previous study indicated that the formation of CH_4 and CH_3OH is through CO intermediate (Hori et al., 2008), which is different from our results.

GN and PyrroN-Doped Graphene

As mentioned above, the pyrrolic N-doped structure has no catalytic activity for CO_2RR. For GN, the free energy increase is the largest among all the N-doped graphene structures (2.55 eV). Thus, the catalytic activity of GN is omitted.

In a word, for the studied structures, the most favorable product is HCOOH, followed by CO and COHOH. In particular, the formation of HCOOH and CO is competitive since the free energy of CO is more thermodynamically favorable by only about 0.20 eV than that of HCOOH. This energy difference is similar to the value of 0.28 eV reported earlier (Liu et al., 2016). In a word, Z-pyN and Z-GN possess the highest catalytic activity toward HCOOH due to the smallest limiting potential of −0.38 and −0.39 V, respectively (**Table 2**), which is lower than −0.44 for PyrroN3 (Liu et al., 2016).

Hydrogen Evolution Reactions

Hydrogen evolution reaction (HER) is the competitive reaction for CO_2RR since the evolution of H would consume the proton–electron pair ($H^+ + e^-$) and passivate the catalytic activity of CO_2RR. For the studied structures, the results showed that Z-pyN-O and Z-pyN have large energetic downhill for the adsorption of H*, indicating the enhanced HER in thermodynamic (**Figure 5**). For Z-GN and A-pyN, they have a negligible free energy barrier (0.03 and 0.04 eV) of H*. For the remaining structures, HER is hindered by large free energy barriers. Therefore, for the most favorable Z-pyN and

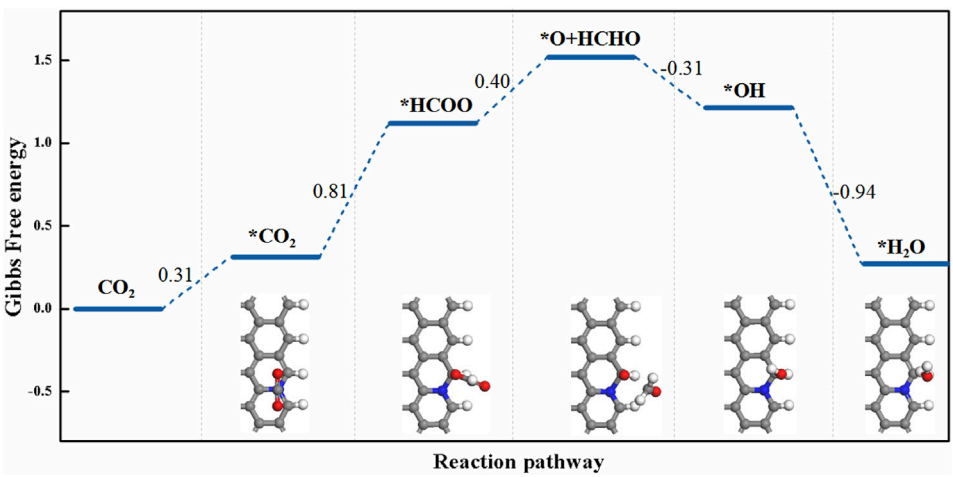

FIGURE 3 | The free energy change for the reaction of $CO_2 + 4H^+ + 4e^- \rightarrow HCHO + H_2O$ on Z-GN.

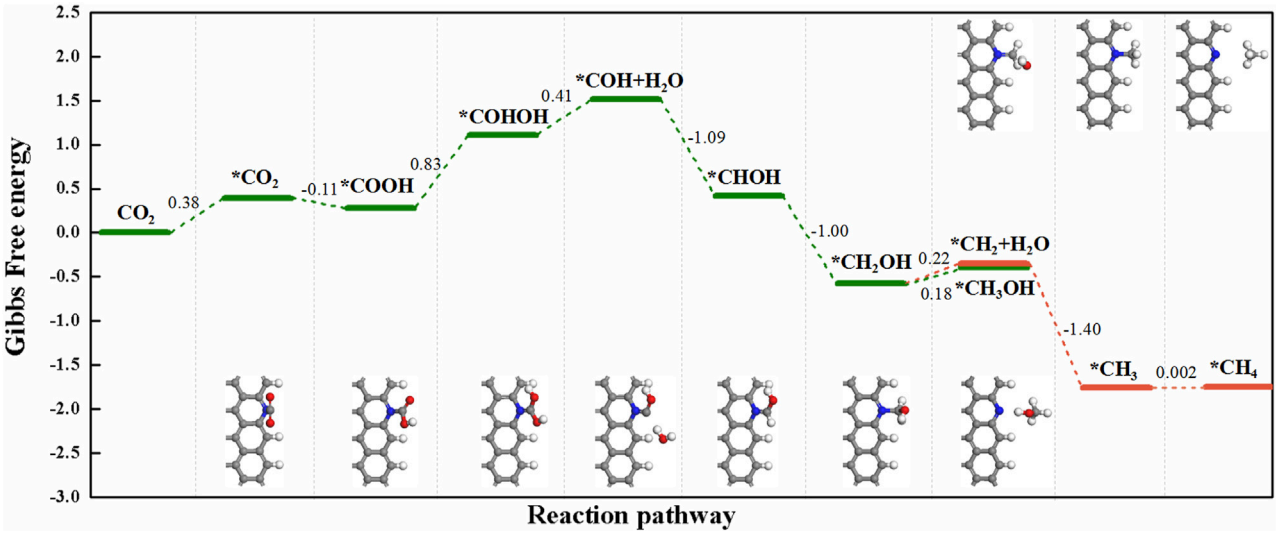

FIGURE 4 | The free energy change for the reaction of $CO_2 + 8H^+ + 8e^- \rightarrow CH_4 + H_2O$ and $CO_2 + 6H^+ + 6e^- \rightarrow CH_3OH + H_2O$ on Z-pyN.

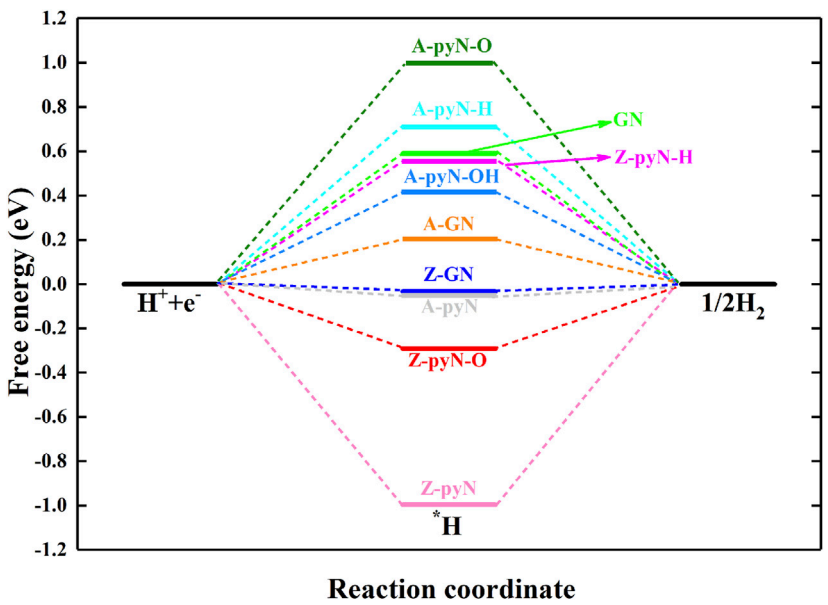

FIGURE 5 | The free energy changes for hydrogen evolution reaction (HER) on various N-doped graphene.

Z-GN, CO_2RR would be suppressed by HER. However, by choosing a suitable electrolyte, the activation energy of HER would be increased. For instance, according to the expression $\Delta G_{pH=}$ 2.303k_BT pH, in which pH = 0 is selected in the above study, ΔG_{pH} = 0.42 eV is obtained for pH = 7.0. Thus, the activation energy of HER on Z-GN would be increased from −0.03 to 0.39 eV, comparable to the free energy barrier of 0.38 eV in the CO_2RR process. Thus, the HER could be suppressed by increasing the pH value for Z-GN. While for Z-pyN, CO_2RR is passivated by too strong HER. In a word, Z-GN could be selected as a promising nonmetal electrocatalyst for CO_2RR in generating HCOOH.

CONCLUSION

We have performed the DFT method to elucidate the reaction mechanism and activity of CO_2RR on 11 types of N-doped graphene catalysts. It indicates that for all the studied structures, the formation of HCOOH is the most favorable, followed by CO.

Among these structures, Z-pyN- and Z-GN-doped graphene exhibit the best catalytic activity for producing HCOOH with free energy barriers of 0.38 and 0.39 eV, respectively. The potential determining step (PDS) is $CO_2 \rightarrow *CO_2$ for Z-pyN and $*CO_2 \rightarrow *COOH$ for Z-GN, respectively. Meanwhile, CO is the competitive product which lies 0.20 eV above HCOOH. For the zigzag pyridinic N-doped graphene, it could also produce CH_3OH and CH_4 as the minor products which need to overcome an energy barrier of 0.83 eV. The minor product for the zigzag graphitic N-doped graphene is HCHO, with an energy barrier of 0.81 eV. However, for Z-pyN, CO_2RR is passivated by too strong HER. Meanwhile, by modifying the pH value of electrolyte, Z-GN could be selected as a promising nonmetal electrocatalyst for CO_2RR in generating HCOOH.

DATA AVAILABILITY STATEMENT

The original contributions presented in the study are included in the article/**Supplementary Material**; further inquiries can be directed to the corresponding author.

AUTHOR CONTRIBUTIONS

The author confirms being the sole contributor to this work and has approved it for publication.

FUNDING

We are grateful for funding support from the National Key R&D Program of China (2019YFA0308000), the Natural Science Foundation of China (no. 21873050), and the Priority Academic Program Development of Jiangsu Higher Education Institutions.

SUPPLEMENTARY MATERIAL

The Supplementary Material for this article can be found online at: https://www.frontiersin.org/articles/10.3389/fchem.2021.734460/full#supplementary-material

REFERENCES

Appel, A. M., Bercaw, J. E., Bocarsly, A. B., Dobbek, H., DuBois, D. L., Dupuis, M., et al. (2013). Frontiers, Opportunities, and Challenges in Biochemical and Chemical Catalysis of CO2Fixation. *Chem. Rev.* 113 (8), 6621–6658. doi:10.1021/cr300463y

Bai, X., Chen, W., Zhao, C., Li, S., Song, Y., Ge, R., et al. (2017). Exclusive Formation of Formic Acid from CO2 Electroreduction by a Tunable Pd-Sn Alloy. *Angew. Chem.* 129 (40), 12387–12391. doi:10.1002/ange.201707098

Blöchl, P. E. (1994). Projector Augmented-Wave Method. *Phys. Rev. B* 50 (24), 17953–17979. doi:10.1103/PhysRevB.50.17953

Cook, T. R., Dogutan, D. K., Reece, S. Y., Surendranath, Y., Teets, T. S., and Nocera, D. G. (2010). Solar Energy Supply and Storage for the Legacy and Nonlegacy Worlds. *Chem. Rev.* 110 (11), 6474–6502. doi:10.1021/cr100246c

Delley, B. (2000). From Molecules to Solids with the DMol3 Approach. *J. Chem. Phys.* 113 (18), 7756–7764. doi:10.1063/1.1316015

Faccio, R., Fernández-Werner, L., Pardo, H., Goyenola, C., Ventura, O. N., and Mombrú, Á. W. (2010). Electronic and Structural Distortions in Graphene Induced by Carbon Vacancies and Boron Doping. *J. Phys. Chem. C* 114 (44), 18961–18971. doi:10.1021/jp106764h

Gao, D., Zhou, H., Wang, J., Miao, S., Yang, F., Wang, G., et al. (2015). Size-Dependent Electrocatalytic Reduction of CO2over Pd Nanoparticles. *J. Am. Chem. Soc.* 137 (13), 4288–4291. doi:10.1021/jacs.5b00046

Geng, D., Chen, Y., Chen, Y., Li, Y., Li, R., Sun, X., et al. (2011). High Oxygen-Reduction Activity and Durability of Nitrogen-Doped Graphene. *Energy Environ. Sci.* 4, 760–764. doi:10.1039/C0EE00326C

Gong, K., Du, F., Xia, Z., Durstock, M., and Dai, L. (2009). Nitrogen-Doped Carbon Nanotube Arrays with High Electrocatalytic Activity for Oxygen Reduction. *Science* 323 (5915), 760–764. doi:10.1126/science.1168049

Grimme, S. (2006). Semiempirical GGA-type Density Functional Constructed with a Long-Range Dispersion Correction. *J. Comput. Chem.* 27 (15), 1787–1799. doi:10.1002/jcc.20495

Holby, E. F., Wu, G., Zelenay, P., and Taylor, C. D. (2014). Structure of Fe-Nx-C Defects in Oxygen Reduction Reaction Catalysts from First-Principles Modeling. *J. Phys. Chem. C* 118 (26), 14388–14393. doi:10.1021/jp503266h

Hori, Y., Kikuchi, K., Kikuchi, S., and Suzuki, S. (1985). Production of Co and Ch4in Electrochemical Reduction of Co2at Metal Electrodes in Aqueous Hydrogencarbonate Solution. *Chem. Lett.* 14 (11), 1695–1698. doi:10.1246/cl.1985.1695

Hori, Y., Kikuchi, K., Murata, A., and Suzuki, S. (1986). Production of Methane and Ethylene in Electrochemical Reduction of Carbon Dioxide at Copper Electrode in Aqueous Hydrogencarbonate Solution. *Chem. Lett.* 15 (6), 897–898. doi:10.1246/cl.1986.897

Hori, Y., Vayenas, C. G., White, R. E., and Gamboa-Aldeco, M. E. (2008). *Electrochemical CO_2 Reduction on Metal Electrodes*. New York: Springer, 89–189. doi:10.1007/978-0-387-49489-0_342

Kang, P., Zhang, S., Meyer, T. J., and Brookhart, M. (2014). Rapid Selective Electrocatalytic Reduction of Carbon Dioxide to Formate by an Iridium Pincer Catalyst Immobilized on Carbon Nanotube Electrodes. *Angew. Chem. Int. Ed.* 53 (33), 8709–8713. doi:10.1002/anie.201310722

Kim, C., Jeon, H. S., Eom, T., Jee, M. S., Kim, H., Friend, C. M., et al. (2015). Achieving Selective and Efficient Electrocatalytic Activity for CO2 Reduction Using Immobilized Silver Nanoparticles. *J. Am. Chem. Soc.* 137 (43), 13844–13850. doi:10.1021/jacs.5b06568

Kim, D., Resasco, J., Yu, Y., Asiri, A. M., and Yang, P. (2014). Synergistic Geometric and Electronic Effects for Electrochemical Reduction of Carbon Dioxide Using Gold-Copper Bimetallic Nanoparticles. *Nat. Commun.* 5, 4948. doi:10.1038/ncomms5948

Kohn, W., and Sham, L. J. (1965). Self-Consistent Equations Including Exchange and Correlation Effects. *Phys. Rev.* 140 (4A), A1133–A1138. doi:10.1103/PhysRev.140.A1133

Kondratenko, E. V., Mul, G., Baltrusaitis, J., Larrazábal, G. O., and Pérez-Ramírez, J. (2013). Status and Perspectives of CO2 Conversion into Fuels and Chemicals by Catalytic, Photocatalytic and Electrocatalytic Processes. *Energ. Environ. Sci.* 6 (11), 3112–3135. doi:10.1039/C3EE41272E

Kresse, G., and Furthmüller, J. (1996b). Efficiency of Ab-Initio Total Energy Calculations for Metals and Semiconductors Using a Plane-Wave Basis Set. *Comput. Mater. Sci.* 6 (1), 15–50. doi:10.1016/0927

Kresse, G., and Furthmüller, J. (1996a). Efficient Iterative Schemes Forab Initiototal-Energy Calculations Using a Plane-Wave Basis Set. *Phys. Rev. B* 54 (16), 11169–11186. doi:10.1103/PhysRevB.54.11169

Kumar, B., Asadi, M., Pisasale, D., Sinha-Ray, S., Rosen, B. A., Haasch, R., et al. (2013). Renewable and Metal-free Carbon Nanofibre Catalysts for Carbon Dioxide Reduction. *Nat. Commun.* 4, 2819. doi:10.1038/ncomms3819

Lee, S., Ocon, J. D., Son, Y.-i., and Lee, J. (2015). Alkaline CO2 Electrolysis toward Selective and Continuous HCOO- Production over SnO2 Nanocatalysts. *J. Phys. Chem. C* 119 (9), 4884–4890. doi:10.1021/jp512436w

Lewis, N. S., Nocera, D. G., and NoceraD, G. (2006). Powering the Planet: Chemical Challenges in Solar Energy Utilization. *Proc. Natl. Acad. Sci.* 103 (43), 15729–15735. doi:10.1073/pnas.0603395103

Li, W., Wu, J., Higgins, D. C., Choi, J.-Y., and Chen, Z. (2012). Determination of Iron Active Sites in Pyrolyzed Iron-Based Catalysts for the Oxygen Reduction Reaction. *ACS Catal.* 2 (12), 2761–2768. doi:10.1021/cs300579b

Lim, R. J., Xie, M., Sk, M. A., Lee, J.-M., Fisher, A., Wang, X., et al. (2014). A Review on the Electrochemical Reduction of CO2 in Fuel Cells, Metal Electrodes and Molecular Catalysts. *Catal. Today* 233, 169–180. doi:10.1016/j.cattod.2013.11.037

Lin, Z., Waller, G. H., Liu, Y., Liu, M., and Wong, C.-p. (2013). 3D Nitrogen-Doped Graphene Prepared by Pyrolysis of Graphene Oxide with Polypyrrole for Electrocatalysis of Oxygen Reduction Reaction. *Nano Energy* 2, 241–248. doi:10.1016/j.nanoen.2012.09.002

Liu, Y., Zhao, J., and Cai, Q. (2016). Pyrrolic-nitrogen Doped Graphene: a Metal-free Electrocatalyst with High Efficiency and Selectivity for the Reduction of Carbon Dioxide to Formic Acid: a Computational Study. *Phys. Chem. Chem. Phys.* 18, 5491–5498. doi:10.1039/C5CP07458D

Lu, Z. (2021). Computational Discovery of Energy Materials in the Era of Big Data and Machine Learning: A Critical Review. *Mater. Rep. Energ.*, 100047. doi:10.1016/j.matre.2021.100047

Lu, Z., Yang, Z., Li, C., Wang, K., Han, J., Tong, P., et al. (2021). Modulating Nanoinhomogeneity at Electrode-Solid Electrolyte Interfaces for Dendrite-Proof Solid-State Batteries and Long-Life Memristors. *Adv. Energ. Mater.* 11 (16), 2003811. doi:10.1002/aenm.202003811

Mathew, K., Kolluru, V. S. C., Mula, S., Steinmann, S. N., and Hennig, R. G. (2019). Implicit Self-Consistent Electrolyte Model in Plane-Wave Density-Functional Theory. *J. Chem. Phys.* 151 (23), 234101. doi:10.1063/1.5132354

Nie, X., Esopi, M. R., Janik, M. J., and Asthagiri, A. (2013). Selectivity of CO2Reduction on Copper Electrodes: The Role of the Kinetics of Elementary Steps. *Angew. Chem. Int. Ed.* 52 (9), 2459–2462. doi:10.1002/anie.201208320

Nørskov, J. K., Rossmeisl, J., Logadottir, A., Lindqvist, L., Kitchin, J. R., Bligaard, T., et al. (2004). Origin of the Overpotential for Oxygen Reduction at a Fuel-Cell Cathode. *J. Phys. Chem. B* 108 (46), 17886–17892. doi:10.1021/jp047349j

Perdew, J. P., Burke, K., and Ernzerhof, M. (1996). Generalized Gradient Approximation Made Simple. *Phys. Rev. Lett.* 77 (18), 3865–3868. doi:10.1103/PhysRevLett.77.3865

Qu, L., Liu, Y., Baek, J.-B., and Dai, L. (2010). Nitrogen-Doped Graphene as Efficient Metal-free Electrocatalyst for Oxygen Reduction in Fuel Cells. *ACS Nano* 4 (3), 1321–1326. doi:10.1021/nn901850u

Ren, D., Deng, Y., Handoko, A. D., Chen, C. S., Malkhandi, S., and Yeo, B. S. (2015). Selective Electrochemical Reduction of Carbon Dioxide to Ethylene and Ethanol on Copper(I) Oxide Catalysts. *ACS Catal.* 5 (5), 2814–2821. doi:10.1021/cs502128q

Shang, Y., Zhao, J.-x., Wu, H., Cai, Q.-h., Wang, X.-g., and Wang, X.-z. (2010). Chemical Functionalization of Pyridine-like and Porphyrin-like Nitrogen-Doped Carbon (CN X) Nanotubes with Transition Metal (TM) Atoms: a Theoretical Study. *Theor. Chem. Acc.* 127 (5-6), 727–733. doi:10.1007/s00214-010-0784-9

Sharma, P. P., Wu, J., Yadav, R. M., Liu, M., Wright, C. J., Tiwary, C. S., et al. (2015). Nitrogen-Doped Carbon Nanotube Arrays for High-Efficiency Electrochemical Reduction of CO2: On the Understanding of Defects, Defect Density, and Selectivity. *Angew. Chem. Int. Ed.* 54 (46), 13701–13705. doi:10.1002/anie.201506062

Sun, X., Kang, X., Zhu, Q., Ma, J., Yang, G., Liu, Z., et al. (2016). Very Highly Efficient Reduction of CO2to CH4using Metal-free N-Doped Carbon Electrodes. *Chem. Sci.* 7, 2883–2887. doi:10.1039/C5SC04158A

Thomas, C. D., Cameron, A., Green, R. E., Bakkenes, M., Beaumont, L. J., Collingham, Y. C., et al. (2004). Extinction Risk from Climate Change. *Nature* 427 (6970), 145–148. doi:10.1038/nature02121

Wang, H., Chen, Y., Hou, X., Ma, C., and Tan, T. (2016). Nitrogen-doped Graphenes as Efficient Electrocatalysts for the Selective Reduction of Carbon Dioxide to Formate in Aqueous Solution. *Green. Chem.* 18, 3250–3256. doi:10.1039/C6GC00410E

Wang, H., Jia, J., Song, P., Wang, Q., Li, D., Min, S., et al. (2017). Efficient Electrocatalytic Reduction of CO2by Nitrogen-Doped Nanoporous Carbon/Carbon Nanotube Membranes: A Step towards the Electrochemical CO2Refinery. *Angew. Chem. Int. Ed.* 56 (27), 7847–7852. doi:10.1002/anie.201703720

Wang, Q., Zhou, Z.-Y., Lai, Y.-J., You, Y., Liu, J.-G., Wu, X.-L., et al. (2014b). Phenylenediamine-Based FeNx/C Catalyst with High Activity for Oxygen Reduction in Acid Medium and its Active-Site Probing. *J. Am. Chem. Soc.* 136 (31), 10882–10885. doi:10.1021/ja505777v

Wang, X., Niu, H., Liu, Y., Shao, C., Robertson, J., Zhang, Z., et al. (2020). Theoretical Investigation on Graphene-Supported Single-Atom Catalysts for Electrochemical CO2 Reduction. *Catal. Sci. Technol.* 10 (24), 8465–8472. doi:10.1039/d0cy01870h

Wang, X., Sun, G., Routh, P., Kim, D.-H., Huang, W., and Chen, P. (2014a). Heteroatom-doped Graphene Materials: Syntheses, Properties and Applications. *Chem. Soc. Rev.* 43, 7067–7098. doi:10.1039/C4CS00141A

Wu, G., More, K. L., Johnston, C. M., and Zelenay, P. (2011). High-Performance Electrocatalysts for Oxygen Reduction Derived from Polyaniline, Iron, and Cobalt. *Science* 332 (6028), 443–447. doi:10.1126/science.1200832

Wu, J., Liu, M., Sharma, P. P., Liu, C. S., Zou, X., Zhou, X. D., et al. (2015). Achieving Highly Efficient, Selective, and Stable CO2 Reduction on Nitrogen-Doped Carbon Nanotubes. *ACS Nano* 9 (5), 5364–5371. doi:10.1021/acsnano.5b01079

Wu, J., Ma, S., Sun, J., Gold, J. I., Tiwary, C., Kim, B., et al. (2016). A Metal-free Electrocatalyst for Carbon Dioxide Reduction to Multi-Carbon Hydrocarbons and Oxygenates. *Nat. Commun.* 7, 13869. doi:10.1038/ncomms13869

Yi, J., Chen, J., Yang, Z., Dai, Y., Li, W., Cui, J., et al. (2019). Facile Patterning of Laser-Induced Graphene with Tailored Li Nucleation Kinetics for Stable Lithium-Metal Batteries. *Adv. Energ. Mater.* 9 (38), 1901796. doi:10.1002/aenm.201901796

Zhang, S., Kang, P., and Meyer, T. J. (2014a). Nanostructured Tin Catalysts for Selective Electrochemical Reduction of Carbon Dioxide to Formate. *J. Am. Chem. Soc.* 136 (5), 1734–1737. doi:10.1021/ja4113885

Zhang, S., Kang, P., Ubnoske, S., Brennaman, M. K., Song, N., House, R. L., et al. (2014b). Polyethylenimine-Enhanced Electrocatalytic Reduction of CO2to Formate at Nitrogen-Doped Carbon Nanomaterials. *J. Am. Chem. Soc.* 136 (22), 7845–7848. doi:10.1021/ja5031529

Zhu, D. D., Liu, J. L., and Qiao, S. Z. (2016). Recent Advances in Inorganic Heterogeneous Electrocatalysts for Reduction of Carbon Dioxide. *Adv. Mater.* 28 (18), 3423–3452. doi:10.1002/adma.201504766

Zhu, W., Metin, Ö., Lv, H., Guo, S., Wright, C. J., Sun, X., et al. (2013). Monodisperse Au Nanoparticles for Selective Electrocatalytic Reduction of CO2 to CO. *J. Am. Chem. Soc.* 135 (45), 16833–16836. doi:10.1021/ja409445p

Zuluaga, S., and Stolbov, S. (2011). Factors Controlling the Energetics of the Oxygen Reduction Reaction on the Pd-Co Electro-Catalysts: Insight from First Principles. *J. Chem. Phys.* 135 (13), 134702. doi:10.1063/1.3643714

Conflict of Interest: The author declares that the research was conducted in the absence of any commercial or financial relationships that could be construed as a potential conflict of interest.